As-bearing new mineral species from Valletta mine, Maira Valley, Piedmont, Italy: III. Canosioite, Ba2Fe3+ (AsO4)2(OH), description and crystal structure

As-bearing new mineral species from Valletta mine, Maira Valley, Piedmont, Italy: III. Canosioite, $Ba_2Fe^{3+}(AsO_4)_2(OH)$, description and crystal structure

F. CÁMARA[1,2]*, E. BITTARELLO[1,2], M.E. CIRIOTTI[3], F. NESTOLA[4], F. RADICA[5], F. MASSIMI[6], C. BALESTRA[7] AND R. BRACCO[8]

[1]Dipartimento di Scienze della Terra, Università degli Studi di Torino, via Tommaso Valperga Caluso 35, I-10125 Torino, Italy

[2]CrisDi, Interdepartmental Centre for the Research and Development of Crystallography, via Pietro Giuria 5, I-10125, Torino, Italy

[3]Associazione Micromineralogica Italiana, via San Pietro 55, I-10073 Devesi-Cirié, Torino, Italy

[4]Dipartimento di Geoscienze, Università degli Studi di Padova, via G. Gradenigo 6, I-35131 Padova, Italy

[5]Dipartimento di Scienze Geologiche, Università degli Studi Roma Tre, largo San Leonardo Murialdo 1, I-00146 Roma, Italy

[6]Dipartimento di Ingegneria Meccanica e Industriale, Università degli Studi Roma Tre, via della Vasca Navale 79, I-00146 Roma, Italy

[7]Associazione Micromineralogica Italiana, via Luigi Delfino 74, I-17017 Millesimo, Savona, Italy

[8]Associazione Micromineralogica Italiana, via Montenotte 18/6, I-17100 Savona, Italy

*correspondent author's e-mail: fernando.camaraartigas@unito.it

Mineralogical Society

This is a 'preproof' accepted article for Mineralogical Magazine.
This version may be subject to change during the production process.
DOI: 10.1180/minmag.2016.080.097

ABSTRACT

The new mineral species canosioite, ideally $Ba_2Fe^{3+}(AsO_4)_2(OH)$, has been discovered in the dump of Valletta mine, Maira Valley, Cuneo Province, Piedmont, Italy. Its origin is probably related to the reaction between ore minerals and hydrothermal fluids. It occurs in reddish-brown granules, subhedral millimetre-size crystals, with pale yellow streak and vitreous lustre. Canosioite is associated with aegirine, baryte, calcite, hematite, bronze Mn-bearing muscovite, unidentified Mn oxides, and unidentified arsenates. Canosioite is biaxial positive with a $2V_{meas}$ = 84(2)º. It is weakly pleochroic with X = brownish yellow, Y = brown, Z = reddish brown, Z > Y > X. Canosioite is monoclinic, $P2_1/m$, with a = 7.8642(4), b = 6.1083(3), c = 9.1670(5) Å, β = 112.874(6)°, V = 405.73(4) Å^3 and Z = 2. Calculated density is 4.943 g/cm^3. The seven strongest diffraction lines of the observed powder XRD pattern are [d in Å, (I), (hkl)]: 3.713 (18)(111), 3.304 (100)(21-1), 3.058 (31)(020), 3.047 (59)(10-3), 2.801 (73)(112), 2.337 (24)(220), 2.158 (24)(12-3). Electron microprobe analyses gave (wt.%): Na_2O 0.06, MgO 0.43, CaO 0.02, NiO 0.02, CuO 0.03, SrO 0.42, BaO 49.36, PbO 1.69, Al_2O_3 1.25, Mn_2O_3 3.89, Fe_2O_3 6.95, Sb_2O_3 0.01, SiO_2 0.03, P_2O_5 0.02, V_2O_5 10.88, As_2O_5 24.64, SO_3 0.01, F 0.02, H_2O 1.61 was calculated on the basis of 1 (OH,F,H_2O) group p.f.u. IR spectroscopy confirmed the presence of OH. The empirical formula calculated on the basis of 9 O a.p.f.u, is $(Ba_{1.92}Pb_{0.05}Sr_{0.02}Na_{0.01})_{\Sigma 2.00}(Fe^{3+}_{0.52}Mn^{3+}_{0.29}Al_{0.15}Mg_{0.06})_{\Sigma 1.02}[(As_{0.64}V_{0.36})_{\Sigma 1.00}O_4]_2[(OH_{0.92}F_{0.01})(H_2O)_{0.07}]$ and the ideal formula is $Ba_2Fe^{3+}(AsO_4)_2(OH)$. The crystal structure was solved by direct methods and found to be isostructural to that of arsenbrackebuschite. The structure model was refined (R_1 2.6%) on the basis of 1245 observed reflections. Canosioite is named after the small municipality of Canosio, where the type locality, the Valletta mine, is situated. The new mineral and name were approved by the IMA CNMNC (IMA2015-030).

This is a 'preproof' accepted article for Mineralogical Magazine.
This version may be subject to change during the production process.
DOI: 10.1180/minmag.2016.080.097

Keywords: canosioite, arsenate, arsenbrackebuschite-group, new mineral species, crystal structure, Valletta, Piedmont, Italy

INTRODUCTION

This is the third of a series of new mineral descriptions of As–bearing minerals from the Valletta mine (Cámara *et al*. 2014, 2015). The sample containing canosioite was collected by one of the authors (CB) in the dumps of Valletta mine, Vallone della Valletta, Canosio municipality, Maira Valley, Cuneo Province, Piedmont, Italy (44°23'54" N, 7°5’37" E, 2560 m asl). Canosioite is named after the small municipality of Canosio, about 80 inhabitants, where the type locality, the Valletta mine, is situated. The new mineral and name were approved by the International Mineralogical Association Commission on New Minerals, Nomenclature and Classification (IMA2015-030).

The holotype material is deposited in the mineralogical collection of the Museo Regionale di Scienze Naturali di Torino, Sezione di Mineralogia, Petrografia e Geologia, via Giovanni Giolitti 36, I–10123 Torino, Italy, catalogue number M/15941.

GEOLOGICAL SETTING AND MINERAL OCCURRENCE

Historical and geological information on the Valletta mine are summarized in Cámara *et al*. (2014). The deposit at Valletta mine has never been studied from a genetic point of view and available geological data for the area are of limited detail. Moreover, the volume of mineralized body is however rather limited on the surface. The mine dumps are the only remains of the former mining activities and consist of dispersed quartzites with quartz veins that contain a large variety of mineral phases rich in arsenic, vanadium, barium and strontium.

DOI: 10.1180/minmag.2016.080.097

The new mineral is strictly associated minerals as almost colourless to brownish aegirine, baryte, calcite, hematite, bronze Mn-bearing muscovite, unidentified Mn oxides, and unidentified Mn arsenates. Other minerals in specimens from the same dump locality are adelite, albite, arseniopleite, azurite, bariopharmacosiderite, berzeliite, braccoite (IMA 2013-093), braunite, coralloite, cryptomelane, diopside, fianelite, fluorapatite, gamagarite, ganophyllite, grandaite (IMA 2013-059), gypsum, hollandite, ilmenite, magnesio-arfvedsonite, magnesio-riebeckite, magnetite, malachite, manganberzeliite, mimetite, neotocite, opal, orthoclase, palenzonaite, phlogopite, pyrobelonite, quartz, ranciéite, richterite, rhodochrosite, rhodonite, rutile, saneroite, talc, tetrahedrite, tilasite, tiragalloite, titanite, tokyoite, wallkilldellite, As-bearing fianelite, a Fe^{3+}/Mn^{3+}-bearing oxy dravite , an uric acid dihydrate-like phase, and some potential new species under study.

MINERALOGICAL CHARACTERIZATION

Appearance and physical properties

Well-formed crystals of canosioite are very rare because of the almost total absence of discernible geodes. We found just two small specimens with glassy opaque reddish-brown subhedral crystals up to about 2.5 x 1 x 1mm in size each. Thanks to the natural etching caused by weathering those crystals were spilling out from a 1.5 cm wide white calcite vein (no UV responses at 356 and 264 nm). Traces of the same phase are also observed in a fracture of calcite, in form of micro granules, still of reddish-brown colour, but in this case transparent.

The type sample containing canosioite is small and consists, almost entirely, of calcite and baryte with some strips of hematite and aegirine likely forming a soft and brownish massive

This is a 'preproof' accepted article for Mineralogical Magazine.
This version may be subject to change during the production process.
DOI: 10.1180/minmag.2016.080.097

material (Figures 1 and 2). Subhedral grained crystals (up to 0.3 mm) form massive aggregates.

Individual crystals are reddish-brown and no twinning was observed. Canosioite is translucent and has a pale yellow streak, a vitreous lustre, and does not fluoresce under SW or LW ultraviolet light. Canosioite is optically biaxial positive with a $2V_{meas.} = 84(2)^{o}$. The values of refractive index were not determined, but the mean refractive index is estimated as 1.9, i.e. well beyond our available experimental range. Canosioite is weakly pleochroic with X = brownish yellow, Y = brown, Z = reddish brown, $Z > Y > X$.

The mineral is brittle. No cleavage or parting are observed. Hardness was measured by nanoindentation by using an Agilent Nano Indenter G200 at the Università di Roma Tre – LIME labs. performed in CSM (continuous stiffness measurement) mode, with a frequency of 45 Hz, amplitude of oscillation 2 nm, constant strain rate of 0.05 s^{-1}, and a maximum penetration depth 1000 nm. Results of hardness and modulus profiles were obtained after averaging over 25 different tests. The instrument was completely re-calibrated before testing by performing a series of indentations on a certified amorphous silica reference sample. Observed elastic modulus is 117.9 ±5.4 GPa (displacement 100-200 nm) and hardness is H: 9.11 ±0.78 GPa (displacement 100-200 nm); Vickers Hardness was calculated from H in order to calculate Mohs hardness, obtaining Mohs hardness of 6-6½. Because the method for obtaining hardness used a continuous variation of the load, it is not easy to provide actual Vickers hardness units. Density was not measured due to the small crystal size. The calculated density obtained from the empirical formula and unit-cell parameters of the single crystal used for the crystal-structure determination is 4.943 g/cm^3.

DOI: 10.1180/minmag.2016.080.097

Chemical data

The chemical composition was determined using a Cameca SX-50 electron microprobe (WDS mode) at the Department of Geosciences (Università di Padova) on a mount obtained by embedding a fragment extracted from the holotype close to the place where the crystal used for the diffraction study was extracted. Major and minor elements were determined at 20 kV accelerating voltage and 20 nA beam current (beam size 2 μm), with 40 to 20 s counting time on both peak and background. X-ray counts were converted to oxide wt% using the PAP correction program supplied by Cameca (Pouchou and Pichoir, 1984, 1985). The crystal studied in the thin section was found to be homogeneous (Figure 2). Elements detected by SEM-EDX were measured with the electron microprobe in WDS mode except potassium which was below detection limits.. H_2O was calculated on the basis of one (OH,F,H_2O) p.f.u. and additional protons (forming therefore H_2O groups) to balance the presence of heterovalent cations; Na^+ at *A*, Mg^{2+} at *M* sites. The average of 4 analyses are given in the Table 1.

The empirical formula, calculated on the basis of 9 O a.p.f.u., is, within rounding errors is $(Ba_{1.92}Pb_{0.05}Sr_{0.02}Na_{0.01})_{\Sigma 2.00}(Fe^{3+}_{0.52}Mn^{3+}_{0.29}Al_{0.15}Mg_{0.06})_{\Sigma 1.02}[(As_{0.64}V_{0.36})_{\Sigma 1.00}O_4]_2[(OH)_{0.92}F_{0.01}(H_2O)_{0.07}]$ and the simplified formula is $(Ba,Pb,Sr,Na)_2(Fe^{3+},Mn^{3+},Al,Mg)[(As,V)O_4]_2[(OH),F,(H_2O)]$. The ideal formula is $Ba_2Fe^{3+}(AsO_4)_2(OH)$, which requires BaO 49.04, Fe_2O_3 12.77, As_2O_5 36.75, H_2O 1.44, total 100 wt%.

Electron microprobe data of an unnamed Ba-Fe arsenate, found at the Sn-In-rich Mangabeira A-type Granite (Central Brazil), are quoted in Moura *et al.* (2007), but these data can probably be better assigned to bariopharmacosiderite than to the new species.

Canosioite is unreactive and insoluble in 2 *M* and 10% HCl, and 65% HNO_3.

Micro-Raman spectroscopy and FTIR

This is a 'preproof' accepted article for Mineralogical Magazine.
This version may be subject to change during the production process.
DOI: 10.1180/minmag.2016.080.097

The Raman spectrum of canosioite (Figure 3) was obtained at the Dipartimento di Scienze della Terra (Università di Torino) using a micro/macro Jobin Yvon Mod. LabRam HRVIS, equipped with a motorized x-y stage and an Olympus microscope. The backscattered Raman signal was collected with 50× objective and the Raman spectrum was obtained for a non-oriented crystal. The 632.8 nm line of an He-Ne laser was used as excitation; laser power (20 mW) was controlled by means of a series of density filters. The minimum lateral and depth resolution was set to few μm. The system was calibrated using the 520.6 cm^{-1} Raman band of silicon before each experimental session. The spectra were collected with multiple acquisitions (2 to 3) with single counting times ranging between 20 and 30 seconds. The spectrum was recorded using the LabSpec 5 program from 100 to 4000 cm^{-1}. Fourier transformed infrared (FTIR, Fig. 5) transmission spectrum (64 scans) recorded using a diamond anvil cell (High Pressure Diamond Optics, Inc.) were obtained with a spectrophotometer Bruker Vertex 70 coupled with a Hyperion 3000 microscope at Centro Conservazione e Restauro "La Venaria Reale" (CCR, Torino Italy) equipped with an MCT detector (Infrared Associates Inc.), working in the spectral range from 4000 to 600 cm^{-1} with an average spectral resolution of 4 cm^{-1}.

The Raman spectrum has confirmed the presence of $(AsO_4)^{3-}$, although it is very difficult to separate the contributions of arsenate from those of vanadate groups. In the region 200-600 cm^{-1}: multiple Raman bands are observed at 234, 282 and 368 cm^{-1} (As^{5+}-O bending vibrations), while bands at 326 cm^{-1} is probably due to V-O bending vibrations (Nakamoto, 1986). Same bands are found in the grandaite ($Sr_2Al(AsO4)_2(OH)_2$) spectrum (Cámara *et al.*, 2014) but are shifted to mostly lower frequencies (213, 308, 347 cm^{-1}). Bands occurring at wavenumbers lower than 200 cm^{-1} correspond to *M*-O and lattice modes (133, 147, 163 and 187 cm^{-1}) according to arsenate vibrations (Myneni *et al.*, 1998 a,b and Nakamoto, 1986). Two bands are also observed at those frequencies in grandaite (120 and 162 cm^{-1}). A weak

This is a 'preproof' accepted article for Mineralogical Magazine.
This version may be subject to change during the production process.
DOI: 10.1180/minmag.2016.080.097

and broad band centred around 480 cm^{-1} is also present, which may be resolved into component bands at 457 and 507 cm^{-1} (As-O) and 478 cm^{-1} (the same for As-O and V-O). Again, that group of bands are also present in grandaite but this time shifted to higher frequencies. In addition grandaite shows bands well resolved at 382 (with shoulder at 386 cm^{-1}), 418 and 425 cm^{-1}. In the region of 600-950 cm^{-1}: weak multiple overlapping bands are observed at 686 and 719 cm^{-1}, not present in grandaite. Three most intense peaks are centred at 838, 862 and 896 cm^{-1} that can correspond to $(AsO_4)^{3-}$ stretching mode, although are similar to those expected for the $(VO_4)^{3-}$ groups. A shoulder at 820 cm^{-1} is probably related to the VO_4 symmetric stretching mode (Farmer, 1974). Very similar band frequencies have been observed for grandaite (Cámara *et al*., 2014) showing its three most intense peaks centred at 833, 857 and 899 cm^{-1} (Fig. 4), although the shoulder at 820 cm^{-1} is not present in agreement with its very low V-content (Cámara *et al*. 2014). FTIR spectrum are less resolved. However, a large convoluted absorption peak is present at ~850 cm^{-1}, with a weak shoulder at ~790 cm^{-1}. Surprisingly, no bands were observed in the range between 2500 and 4000 cm^{-1} in the Raman spectrum. The absence of strong bands with frequencies higher than 1000 cm^{-1} would indicate the absence of OH groups in canosioite. Same difficulties in observing bands in the range between 2500 and 4000 cm^{-1} of the Raman spectrum were also found in grandaite (Cámara *et al*., 2014). However, the FTIR spectrum in grandaite showed the presence of broad bands centred at ~3150 cm^{-1} and the absence of any discernible clear absorption at ~1650 cm^{-1}, thus confirming the presence of hydrogen as hydroxyl groups but not of (H_2O) as proposed for arsenbrackebuschite (Fig. 5). The trace amount of F detected in the electron microprobe analysis and, on the basis of crystal structure refinement (see later on) we consider that (OH) groups are also present in canosioite.

X–ray diffraction

This is a 'preproof' accepted article for Mineralogical Magazine.
This version may be subject to change during the production process.
DOI: 10.1180/minmag.2016.080.097

198 Powder X–ray diffraction pattern of canosioite was obtained at CrisDi (Interdepartmental
199 Centre for the Research and Development of Crystallography, Torino, Italy) using an Oxford
200 Gemini R Ultra diffractometer equipped with a CCD area detector, with graphite-
201 monochromatized Mo*K*α radiation. Indexing of the reflections was based on a calculated
202 powder pattern obtained from the structural model, using the software LAZY PULVERIX
203 (Yvon *et al.*, 1977). Experimental and calculated data are reported in Table 2. The unit-cell
204 parameters refined from the powder data with the software GSAS (Larson and Von Dreele,
205 1994) are a = 7.871(3), b = 6.117(2), c = 9.158(5) Å, β = 112.80(3)° and V = 405.9(3) Å^3.
206 Single-crystal X–ray diffraction data were collected using an Oxford Gemini R Ultra
207 diffractometer equipped with a CCD area detector at CrisDi (Università di Torino) using
208 graphite-monochromatized Mo*K*α radiation (λ = 0.71073 Å). A crystal fragment of 0.1 × 0.05
209 × 0.06 mm, showing sharp optical extinction behaviour was used for collecting intensity data.
210 No crystal twinning was observed. Crystal data and experimental details are reported in Table
211 3.
212 The intensities of 2505 reflections with $-11 < h < 9$, $-9 < k < 8$, $-11 < l < 13$ were collected
213 to 64.4° 2θ using 1° frame width and an integration time of 5.5 and 22 s (retakes). We
214 collected 3 ω scans, with a total of 207 frames and a detector crystal distance of 55 mm. Data
215 were integrated and corrected for Lorentz and polarization background effects, using the
216 package CrysAlisPro, Agilent Technologies, Version 1.171.36.20 (release 27-06-2012
217 CrysAlis171.36.24). Refinement of the unit-cell parameters was based on 1471 measured
218 reflections. At room temperature, the unit-cell parameters are a = 7.8642(4), b = 6.1083(3), c
219 = 9.1670(5) Å, β = 112.874(6)°, V = 405.73(4) Å^3, space group $P2_1/m$, Z = 2. The a:b:c ratio
220 is 1.288:1:1.501. A total of 1405 independent reflections were collected and the structure was
221 solved and refined by means of the SHELX set of programs (Sheldrick, 2008). Scattering
222 curves for neutral atoms were taken from International Tables for Crystallography (Wilson,

DOI: 10.1180/minmag.2016.080.097

1992). Structure was refined starting from the atom coordinates of grandaite (Cámara *et al*. 2014). At convergence, a residue in the Fourier difference close to O7 was interpreted as a proton and was added to the model. Hydrogen atom coordinates and isotropic displacement parameter were refined without constraints. Refinement converged to R_1 = 2.58% for 1245 observed reflections with $F_o > 4\sigma(F_o)$ and and 3.30% for all 1405 data and 88 parameters without restraints.

Tables 4, 5 and 6 report displacement parameters, the atomic coordinates, and selected bond distances and angles respectively for canosioite. Bond valence calculations using the parameters of Brown (1981) are reported in Table 7. Tables of structure factors and the CIF file have been deposited with the Principal Editor of Mineralogical Magazine and are available from www.minersoc.org/pages/e_journals/dep_mat_mm.html

DESCRIPTION OF THE STRUCTURE

Structure model

The crystal structure of canosioite (Fig. 6) is isostructural with those of members of the brackebuschite supergruop with the general formula of $A_2{}^{VI}M(^{IV}TO_4)_2X$, where $A = Pb^{2+}$, Ba^{2+}, Sr^{2+}, Ca^{2+}, $M = Fe^{3+}$, Al^{3+}, Mn^{3+}, Zn^{2+}, Fe^{2+}, Cu^{2+}, $T = As^{5+}$, V^{5+}, P^{5+}, S^{6+}, $X = OH^-$, F^-, H_2O: chains of $[M^{3+,2+}(T^{5+}O_4)_2X]$ units are connected through interstitial divalent cations (Pb, Sr, Ba for arsenbrackebuschite, grandaite and canosioite, respectively) in the *A* sites [*A*(1) and *A*(2)] (Fig. 4). In canosioite, the interstitial sites *A*(1) and *A*(2) are occupied almost exclusively by Ba and very minor Pb and Sr. The M^{3+} octahedron is occupied dominantly by Fe^{3+} in canosioite, but significant amount of Mn^{3+} and Al are also present, It shares edges with other *M* octahedra forming a chain along [010]. The shared edge has one anion that, depending on the charge of the cation at the octahedron in each mineral species belonging to the group, can be an OH group or a H_2O molecule, and the other anion is shared with the apex of a $T^{5+}O_4$

This is a 'preproof' accepted article for Mineralogical Magazine.
This version may be subject to change during the production process.
DOI: 10.1180/minmag.2016.080.097

248 tetrahedron [the *T*(1) site]. The remaining four anions coordinating the octahedron are linked
249 to the edge of another $T^{5+}O_4$ tetrahedron (the *T*(2) site) alternating in both sides. Vanadium is
250 frequently present and it is disordered among *T*(1) and *T*(2) sites. It is expected a complete
251 solid solution between canosioite and gamagarite $Ba_2Fe^{3+}(VO_4)_2(OH)$.

252 The interstitial sites in canosioite are almost fully occupied by Ba, with 0.05 apfu of
253 Pb at *A*(1) and 0.02 apfu of Sr at *A*(2). V is not dominant at *T* sites and is distributed among
254 both sites but preferentially at *T*(1), which is also slightly larger and more distorted (Table 6).
255 The *T*(1) is also more distorted in grandaite (Cámara *et al.*, 2014), but it is not in
256 arsenbrackebuschite, which has a larger and more distorted *T*(2) site (Hofmeister and
257 Tillmanns, 1978), probably due to the distorted coordination of lead at the *A*(1,2) sites.
258
259 **Hydrogen bonding**
260 Moderate hydrogen bonding is suggested in the canosioite. An inspection of Table 7 shows
261 that there is one oxygen site with bond valence incidence < 1.5 v.u: O(7). There is one short
262 acceptor-donor distance corresponding to a moderate hydrogen bond [O(7)…O(5) =
263 2.878(10) Å, Table 6]. Using the relation $\nu(cm^{-1}) = 3592-304\times10^{9}\cdot\exp(-d(O\ldots O)/0.1321)$
264 (Libowitzky, 1999), we should expect (OH) stretching bands at ~3380 cm^{-1}. Frequencies at
265 ca. 3150 cm^{-1} are observed in the FTIR spectrum of canosioite (Fig. 5). The positions of one
266 hydrogen atom was observed in the Fourier-difference maps at convergence and was added to
267 the model. In particular, the position observed for the H(7) atom shows a bond with oxygen at
268 the O(7) anion site (0.79(1) Å) with a short H(7)…O(5) distance of 2.017(10) Å. The
269 presence of divalent cations at *M* sites and of monovalent cations at the *A*(1,2) sites must be
270 charge balanced with higher charge at *T*(1,2) sites or can be compensated with some (H_2O)
271 replacing (OH) groups at O(7) as proposed in arsenbrackebuschite (Hofmeister and
272 Tillmanns, 1978). For that reason, 0.07 (H_2O) pfu were calculated (see chemistry section).

This is a 'preproof' accepted article for Mineralogical Magazine.
This version may be subject to change during the production process.
DOI: 10.1180/minmag.2016.080.097

However, the occupancy of the second proton bonded to the O(7) is far too low to be observed in a Fourier-difference map or to be detected with FTIR with a crushed grain in a diamond anvil cell. It is worth noting that the acceptor oxygen at O(5) site is undersaturated even after calculating the contribution from the hydrogen bond (bond valence incidence of 1.71 v.u., Table 7). A similar situation was also observed in grandaite by Cámara *et al.* (2014). In addition, the equivalent displacement parameter for this atom is the highest (ca. twice all the other anions but O(3)). This reflects a stressed topology that may explain the observed higher distortion at the *T*(1) site. Moreover, the hydrogen bonds are perpendicular to the (-101) plane (shown in pink in Figure 6b), which limits the junction of the $[M^{3+,2+}(T^{5+}O_4)_2X]$ units and that includes the *A*(1) sites as well as the O(3) and O(5) anion sites. We hypothesize that this could be a particular weak plane in the structure of these compounds, although no parting has been observed (probably due to the scarcity of material).

RELATED MINERALS

Canosioite, $Ba_2Fe^{3+}(AsO_4)_2(OH)$, is the As-dominant analogue of gamagarite, $Ba_2Fe^{3+}(VO_4)_2(OH,H_2O)$ and the Ba-dominant analogue of arsenbrackebuschite, $Pb_2Fe^{3+}(AsO_4)_2(OH,H_2O)$. It is the first Ba member of the arsenbrackebuschite group of the brackebuschite supergroup (Table 8). Group nomenclature follows IMA rules (Mills et al. 2008). Subgroups are divided on the basis of the charge species dominance at the *T* sites. The crystal chemistry of this supergroup is under study as part of a broader project. The observed composition with a significant amount of Mn^{3+} at the *M* site opens the possibility for a possible end-member As-dominant analogue of tokyoite $Ba_2Mn^{3+}(VO_4)_2(OH)$. We have reported a comparison of the properties of the members of the arsenbrackebuschite group in Cámara *et al.*, (2014). In terms of lattice parameters, canosioite is the one showing the largest cell volume among arsenbrackebuschite group minerals: 405.73(4) $Å^3$ versus 391.2, 384,2(4)

DOI: 10.1180/minmag.2016.080.097

298 and 366.62(4) $Å^3$, for arsenbrackebuschite, feinglosite and grandaite, respectively. This is
299 mostly due to the increment of all three lattice parameters. Compared to arsenbrackebuschite,
300 canosioite has larger cell parameters due to the substitution of lead by larger barium. In the
301 Strunz System (Strunz and Nickel, 2001) canosioite fits in subdivision 8.B.G, phosphates, *etc*.
302 with additional anions, without H_2O, with medium-sized and large cations (OH, *etc*.).
303

304 **ACKNOWLEDGMENTS**

305 The careful review of Peter Leverett and two anonymous reviewer are thanked. Authors
306 wish to thank Bruno Lombardo (CNR-IGG- Torino), Gian Carlo Piccoli, Paolo Bosio and
307 Aldo Marino for their assessment support in field work at Valletta. Marco Nervo (Centro
308 Conservazione e Restauro "La Venaria Reale", Torino Italy) and Tommaso Poli (University
309 of Torino) are thanked for granting access to the FTIR facilities. Raul Carampin (CNR-IGG-
310 Padova, Italy) is thanked for his support on the WDS analysis. FC and EB thank the MIUR
311 and the AMI for the co-funding of a research contract for EB for the year 2013-2014.
312

313 **REFERENCES**

314 Abraham, K., Kautz, K., Tillmanns, E. and Walenta, K. (1978) Arsenbrackebuschite,
315 $Pb_2(Fe,Zn)(OH,H_2O)[AsO_4]_2$, a new arsenate mineral. *Neues Jahrbuch für Mineralogie,*
316 *Monatshefte*, 193-196.

317 Basso, R., Palenzona, A. and Zefiro, L. (1987) Gamagarite: new occurrence and crystal
318 structure refinement. *Neues Jahrbuch für Mineralogie, Monatshefte*, 295-304.

319 Bideaux, R.A., Nichols, M.C., and Williams, S.A. (1966) The arsenate analog of tsumebite, a
320 new mineral. *American Mineralogist*, **51**, 258-259.

DOI: 10.1180/minmag.2016.080.097

321 Brackebusch, L., Rammelsberg, C., Doering, A. and Websky, M. (1883) Sobre los vanadatos
322 naturales de las provincias de Córdoba y San Luis (República Argentina). *Boletín de la*
323 *Academia Nacional de Ciencias (Córdoba)*, **5**, 439-524.
324 Brown, I.D. (1981) The bond-valence method: an empirical approach to chemical structure
325 and bonding. Pp. 1-30 in: *Structure and Bonding in Crystals* II, (M. O'Keeffe and A.
326 Navrotsky, editors). Academic Press, New York.
327 Brunet, F., Gebert, W., Medenbach, O. and Tillmanns, E. (1993) Bearthite, $Ca_2Al[PO_4]_2(OH)$,
328 a new mineral from high-pressure terranes of the western Alps. *Schweizerische*
329 *Mineralogische und Petrographische Mitteilungen*, **73**, 1-9.
330 Brunet, F. and Chopin, C. (1995) Bearthite, $Ca_2Al(PO_4)_2OH$: stability, thermodynamic
331 properties and phase relations. *Contributions to Mineralogy and Petrology*, **121**, 258-266.
332 Busz, K. (1912) Tsumebit, ein neues Mineral von Otavi und Zinnsteinkristalle. *Deutschen*
333 *Naturforscher und Årtze in Münster*, **84**, 230-230 (in German).
334 Cámara, F., Ciriotti, M.E., Bittarello, E., Nestola, F., Bellatreccia, F., Massimi, F., Radica, F.,
335 Costa, E., Benna, P. and Piccoli, G.C. (2014) Arsenic-bearing new mineral species from
336 Valletta mine, Maira Valley, Piedmont, Italy: I. Grandaite, $Sr_2Al(AsO_4)_2(OH)$,
337 description and crystal structure. *Mineralogical Magazine*, **78**, 757-774.
338 Cámara, F., Bittarello, E., Ciriotti, M.E., Nestola, F., Radica, F., Marchesini, M. (2015) As-
339 bearing new mineral species from Valletta mine, Maira Valley, Piedmont, Italy: II.
340 Braccoite, $NaMn^{2+}_5$ $[Si_5AsO_{17}(OH)](OH)$, description and crystal structure.
341 *Mineralogical Magazine*, **79**, 171-189.
342 Clark, A.M., Criddle, A.J., Roberts, A.C., Bonardi, M. and Moffatt, E.A. (1997) Feinglosite, a
343 new mineral related to brackebuschite, from Tsumeb, Namibia. *Mineralogical Magazine*, **61**,
344 285-289.

DOI: 10.1180/minmag.2016.080.097

345 de Villiers, J.E. (1943) Gamagarite, a new vanadium mineral from the Postmasburg
346 manganese deposits. *American Mineralogist*, **28**, 329-335.
347 Donaldson, D.M. and Barnes, W.H. (1955) The structures of the minerals of the descloizite
348 group and adelite groups: III – brackenbuschite. *American Mineralogist*, **40**, 597-613.
349 Fanfani, L. and Zanazzi, P.F. (1967) Structural similarities of some secondary lead minerals.
350 *Mineralogical Magazine*, **36**, 522-529.
351 Farmer V.C. (1974) The Infrared Spectra of Minerals. Mineralogical Society, London, 539
352 pp.
353 Foley, J.A., Hughes, J.M. and Lange, D. (1997) The atomic arrangement of brackebuschite,
354 redefined as $Pb_2(Mn^{3+},Fe^{3+})(VO_4)_2(OH)$, and comments on Mn^{3+} octahedra. *Canadian*
355 *Mineralogist*, **35**, 1027-1033.
356 González del Tánago, J., La Iglesia, Á., Rius, J. and Fernández Santín, S. (2003) Calderónite,
357 a new lead-iron-vanadate of the brackebuschite group. *American Mineralogist*, **88**, 1703-
358 1708.
359 Harlow, G.E., Dunn, P.J. and Rossman, G.R. (1984) Gamagarite: a re-examination and
360 comparison with brackebuschite-like minerals. *American Mineralogist*, **69**, 803-806.
361 Hofmeister, W. and Tillmanns, E. (1978) Strukturelle Untersuchungen an
362 Arsenbrackebuschit. *Tschermaks Mineralogische und Petrographische Mitteilungen*, **25**,
363 153-163 (in German).
364 Kampf, A.R., Adams, P.M., Nash, B.P., and Marty, J. (2015) Ferribushmakinite,
365 $Pb_2Fe^{3+}(PO_4)(VO_4)(OH)$, the Fe^{3+} analogue of bushmakinite from the Silver Coin mine,
366 Valmy, Nevada. *Mineralogical Magazine*, **79**, 661-669.
367 Larson, A.C. and Von Dreele, R.B. (1994) *General Structure Analysis System (GSAS)*. Los
368 Alamos National Laboratory Report LAUR, 86-748.

DOI: 10.1180/minmag.2016.080.097

Libowitzky, E. (1999) Correlation of OH stretching frequencies and O–H…O hydrogen bond lengths in minerals. *Monatshefte für Chemie*, **130**, 1047–1059.

Matsubara, S., Miyawaki, R., Yokoyama, K., Shimizu, M. and Imai, H. (2004) Tokyoite, $Ba_2Mn^{3+}(VO_4)_2(OH)$, a new mineral from the Shiromaru mine, Okutama, Tokyo, Japan. *Journal of Mineralogical and Petrological Sciences*, **99**, 363-367.

Mills, S.J., Hatert, F., Nickel, E.H. and Ferraris, G. (2009) The standardisation of mineral group hierarchies: application to recent nomenclature proposals. *European Journal of Mineralogy*, **21**, 1073-1080.

Moore, P.B., Irving, A.J. and Kampf, A.R. (1975) Foggite, $CaAl(OH)_2(H_2O)[PO_4]$; goedkinite, $(Sr,Ca)_2Al(OH)[PO_4]_2$; and samuelsonite $(Ca,Ba)Fe^{2+}{}_2Mn^{2+}{}_2Ca_8Al_2(OH)_2[PO_4]_{10}$: Three new species from the Palermo No. 1 Pegmatite, North Groton, New Hampshire. *American Mineralogist*, **60**, 957-964.

Moura, M.A., Botelho, N.F., Carvalho de Mendonça, F. (2007) The indium-rich sulfides and rare arsenates of the mineralized Mangabeira A-type granite, Central Brazil. Canadian Mineralogist, 45, 485-496.

Myneni, S.C.B., Traina, S.J., Waychunas, G.A. and Logan, T.J. (1998a) Experimental and Theoretical Vibrational Spectroscopic Evaluation of Arsenate coordination in Aqueous solutions and Solids. *Geochimica et Cosmochimica Acta*, **62**, 3285-3300.

Myneni, S.C.B., Traina, S.J., Waychunas, G.A. and Logan, T.J. (1998b): Vibrational spectroscopy of functional group chemistry and arsenate coordination in ettringite. *Geochimica et Cosmochimica Acta*, **62**, 3499-3514.

Nakamoto, K. (1986) *Infrared and Raman Spectra of Inorganic and Coordination Compounds*. Wiley, New York, 432 pp.

Nichols, M.C. (1966): The structure of tsumebite. *American Mineralogist*, **51**, 267-267.

This is a 'preproof' accepted article for Mineralogical Magazine.
This version may be subject to change during the production process.
DOI: 10.1180/minmag.2016.080.097

393 Pekov, I.V. (2007): New minerals from former Soviet Union countries, 1998-2006: new
394 minerals approved by the IMA Commission on New Minerals and Mineral Names.
395 *Mineralogical Almanac*, **11**, 9-51.
396 Pekov, I.V., Kleimenov, D.A., Chukanov, N.V., Yakubovich, O.V., Massa, W., Belakovskiy,
397 D.I. and, Pautov, L.A. (2002) Bushmakinite $Pb_2Al(PO_4)(VO_4)(OH)$, a new mineral of the
398 brackebuschite group from oxidized zone of Berezovskoye gold deposit, the Middle
399 Urals. *Zapiski Vserossijskogo Mineralogicheskogo Obshchestva*, **131**(2), 62-71 (in
400 Russian).Piccoli, G.C. (2002): *Minerali delle Alpi Marittime e Cozie Provincia di Cuneo*.
401 Amici del Museo "F. Eusebio" – Alba, Ed., Alba, Cuneo, 366 pp. [147-148] (in Italian).
402 Pouchou, J.L. and Pichoir, F. (1984) A new model for quantitative analysis: Part I.
403 Application to the analysis of homogeneous samples. *La Recherche Aerospatiale*, **3**, 13-
404 38.
405 Pouchou, J.L. and Pichoir, F. (1985) `PAP' φ(ρZ) correction procedure for improved
406 quantitative microanalysis. *In Microbeam Analysis* (J.T. Armstrong, Ed.), San Francisco
407 Press, San Francisco, California (104-106).
408 Rammelsberg, C. (1880) Ueber die vanadinerze aus dem Staat Córdoba in Argentinien.
409 *Zeitschrift der Deutschen Geologischen Gesellschaft*, **32**, 708-713 (in German).
410 Robinson, K., Gibbs, G.V. and Ribbe, P.H. (1971) Quadratic elongation: a quantitative
411 measure of distortion in coordination polyhedra. *Science*, **172**, 567-570.
412 Rosicky, V. (1912): Preslit, ein neues Mineral von Tsumeb in Deutsch-Südwestafrika.
413 *Zeitschrift für Krystallographie und Mineralogie*, **51**, 521-526 (in German).
414 Roth, P. (2007) Bearthite. *In*: *Minerals first discovered in Switzerland and minerals named*
415 *after Swiss individuals*. Kristallografik Verlag, Achberg (Germany), 239 pp. [44-45].
416 Sheldrick, G.M. (2008) A short history of SHELX. *Acta Crystallographica*, **A64**,112-122.

417 Spencer, L.J. (1913) A (sixth) list of new mineral names. *Mineralogical Magazine*, **16**, 352-
418 378.
419 Strunz, H. and Nickel, E.H. (2001) *Strunz Mineralogical Tables. Chemical Structural Mineral*
420 *Classification System. 9th Edition*. E. Schweizerbart, Ed., Stuttgart (Germany), 870 pp.
421 Vésignié, J.P.L. (1935) Présentation d'échantillons. *Bulletin de la Société Française de*
422 *Minéralogie*, **58**, 4-5 (in French).
423 Williams, S.A. (1973) Heyite, $Pb_5Fe_2(VO_4)_2O_4$, a new mineral from Nevada. *Mineralogical*
424 *Magazine*, **39**, 65-68.
425 Wilson, A.J.C. (editor) (1992) International Tables for Crystallography. Volume C:
426 Mathematical, Physical and Chemical Tables. Kluwer Academic Publishers, Dordrecht,
427 The Netherlands.
428 Yakubovich, O.V., Massa, W. and Pekov, I.V. (2002) Crystal structure of the new mineral
429 bushmakinite, $Pb_2\{(Al,Cu)[PO_4][(V,Cr,P)O_4](OH)\}$. *Doklady Earth Sciences*, **382**, 100-
430 105 (in Russian).
431 Yvon, K., Jeitschko, W. and Parthé, E. (1977) LAZY PULVERIX, a computer program, for
432 calculating Xray and neutron diffraction powder patterns. *Journal of Applied*
433 *Crystallography*, **10**, 73-74.
434 Zubkova, N.V., Pushcharovsky, D.Y., Giester, G., Tillmanns, E., Pekov, I.V. and Kleimenov,
435 D.A. (2002) The crystal structure of arsentsumebite, $Pb_2Cu[(As,S)O_4]_2(OH)$. *Mineralogy*
436 *and Petrology*, **75**, 79-88.
437

DOI: 10.1180/minmag.2016.080.097

438 **Figures captions**

439

440 **Figure 1**. Reddish-brown granules or subhedral crystals of canosioite on calcite (FoV 5 mm)
441 (collection and photo R. Bracco).

442

443 **Figure 2**. Backscattered electron image of a thin section of canosioite (light grey) in
444 association with baryte (medium grey).

445

446 **Figure 3**. Raman spectra of canosioite showing the 100-4000 cm^{-1} range and the region and
447 between 100 and 1200 cm^{-1} enlarged.

448

449 **Figure 4**. Raman spectrum of canosioite compared to that of grandaite (Cámara *et al*., 2014)
450 in the 100-1100 cm^{-1} region.

451

452 **Figure 5**. FTIR spectrum of canosioite in the 100-4000 cm^{-1} region and between 100 and
453 1200 cm^{-1}.

454

455 **Figure 6**. Detail of the canosioite structure showing: a) the chains of Fe^{3+} octahedral
456 (projected onto [010]), AsO_4 groups and interstitial large cations; b) a detail of the (-101)
457 plane perpendicular to the hydrogen bonds. Orange: As tetrahedra (dark *T*(1), light *T*(2));
458 blue: Fe^{3+} octahedra; green: Ba sites (dark *A*(1), light *A*(2)); white: H sites; red: oxygen sites.
459 O-H…O bond showed with a dashed black line. Thermal displacement ellipsoids shown at
460 95% probability.

461

DOI: 10.1180/minmag.2016.080.097

TABLES

Table 1

	Wt.%	Range	stand. dev.	Probe standard (crystal, line)
Na_2O	0.06	0.00-0.12	0.05	albite Amelia (TAP, *Kα*)
MgO	0.43	0.35-0.56	0.09	synthetic periclase (TAP,*Kα*)
CaO	0.02	0.00-0.03	0.01	diopside (TAP, *Kα*)
NiO	0.02	0.00-0.05	0.02	NiO (LIF, *Kα*)
CuO	0.03	0.00-0.08	0.04	metallic Cu (LIF, *Kα*)
SrO	0.42	0.26-0.77	0.25	celestine (PET, *Lα*)
BaO	49.36	48.86-50.27	0.65	baryte (LIF, *Lα*)
PbO	1.69	1.47-2.02	0.26	Pb (PET, *Mα*)
Al_2O_3	1.25	1.23-1.27	0.02	corundum (TAP, *Kα*)
Mn_2O_3	3.89	3.65-4.19	0.22	$MnTiO_3$ (LIF, *Kα*)
Fe_2O_3	6.95	6.60-7.18	0.25	Fe_2O_3 (LIF, *Kα*)
Sb_2O_3	0.01	0.00-0.04	0.02	Sb_2S_3 (PET, *Lα*)
SiO_2	0.03	0.01-0.06	0.02	diopside (TAP, *Kα*)
P_2O_5	0.02	0.00-0.08	0.04	apatite (TAP, *Kα*)
V_2O_5	10.88	8.80-9.48	0.48	vanadinite (LIF, *Kα*)
As_2O_5	24.64	24.06-25.34	0.46	synthetic AsGa (TAP, *Lα*)
SO_3	0.01	0.00-0.04	0.02	sphalerite (PET, *Kα*)
F	0.02	0.00-0.09	0.05	fluorite (TAP, *Kα*)
H_2O	1.61	1.58-1.68		
O = F	-0.01	0.00-0.04	0.05	
Total	101.34			

Table 1. Analytical data for canosioite

DOI: 10.1180/minmag.2016.080.097

Table 2.

h	*k*	*l*	d_{obs}(Å)	d_{calc} (Å)	Int.$_{(obs)}$	Int.$_{(calc)}$
1	1	0	4.674	4.670	7	6
1	**1**	**1**	**3.713**	**3.712**	**18**	**16**
0	1	2	3.470	3.474	9	5
2	**1**	**$\bar{1}$**	**3.304**	**3.304**	**100**	**100**
0	**2**	**0**	**3.058**	**3.054**	**31**	**47**
1	**0**	**$\bar{3}$**	**3.047**	**3.056**	**59**	**69**
2	1	$\bar{2}$	3.037	3.039	13	11
2	0	1	2.941	2.941	11	10
0	2	1	2.874	2.872	15	10
1	2	0	2.817	2.814	9	6
1	**1**	**2**	**2.801**	**2.802**	**73**	**60**
2	1	1	2.651	2.650	8	12
2	1	$\bar{3}$	2.553	2.557	13	9
2	**2**	**0**	**2.337**	**2.335**	**24**	**24**
1	**2**	**$\bar{3}$**	**2.158**	**2.160**	**24**	**36**
3	0	1	2.115	2.115	11	18
3	1	$\bar{4}$	1.921	1.924	18	18
4	0	$\bar{3}$	1.893	1.895	7	8
2	3	$\bar{1}$	1.809	1.808	16	13
1	1	4	1.763	1.765	9	5
3	2	1	1.740	1.739	15	20
1	3	2	1.712	1.711	14	16
4	2	$\bar{2}$	1.652	1.652	13	10
1	2	$\bar{5}$	1.553	1.556	13	9

*Only reflections with $I_{cal} > 6\sigma(I_{cal})$ are listed

Table 2. X-ray powder diffraction data for canosioite.* The seven strongest reflections are reported in bold

DOI: 10.1180/minmag.2016.080.097

Table 3.

Crystal system	Monoclinic
Space group	$P2_1/m$
Unit–cell dimensions	
a (Å)	7.8642(4)
b (Å)	6.1083(3)
c (Å)	9.1670(5)
β (°)	112.874(6)
V (Å^3)	405.73(4)
Z	2
μ (mm^{-1})	16.71
F(000)	525
D_{calc} (g cm^{-3})	4.943
Crystal size (mm)	0.10 × 0.05 × 0.06
Radiation type	Mo $K\alpha$ (0.71073 Å)
Temperature (K)	298
θ–range for data collection (º)	4.1-32.2
R_{int}	0.026
Reflections collected	2505
Independent reflections	1405
F_o>4σ(F)	1245
Refinement method	least-squares matrix: full
No. of refined parameters	88
Final R_{obs} (%) all data	3.3
R_1(%) Fo>4σ(F)	2.6
wR_2 (%) F_o>4σ(F)	5.5
Highest peak/deepest hole (e Å^{-3})	1.16/-1.31
Goodness of fit on F^2	1.017

Table 3. Crystal data and summary of parameters describing data collection and refinement for canosioite

This is a 'preproof' accepted article for Mineralogical Magazine.
This version may be subject to change during the production process.
DOI: 10.1180/minmag.2016.080.097

Table 4.

Site	Mult.	Occ.	*x*/*a*	*y*/*b*	*z*/*c*	U_{eq}
T(1)	2*e*	0.412(12)As 0.588(12)V	0.43719(9)	¼	0.17014(7)	0.0080(2)
T(2)	2*e*	0.686(14)As 0.314(14)V	0.04486(7)	¼	0.33357(6)	0.00664(19)
M	2*a*	0.233(9)Mg 0.767(9)Fe	0	0	0	0.0078(2)
A(1)	2*e*	0.957(13)Ba 0.043(13)Sr	0.26494(4)	¼	0.75236(4)	0.01679(12)
A(2)	2*e*	0.906(13)Ba 0.094(13)Sr	0.67834(4)	¼	0.58533(4)	0.01018(10)
O(1)	4*f*		−0.0055(4)	0.5185(4)	0.7815(3)	0.0144(6)
O(2)	2*e*		0.2660(5)	¼	0.4567(4)	0.0186(9)
O(3)	2*e*		0.9115(6)	¼	0.4349(5)	0.0245(10)
O(4)	4*f*		0.4942(4)	0.0281(4)	0.2873(3)	0.0173(6)
O(5)	2*e*		0.5514(6)	¼	0.0489(5)	0.0325(12)
O(6)	2*e*		0.1986(5)	¼	0.0466(4)	0.0168(8)
O(7)	2*e*		0.8295(5)	¼	0.9316(4)	0.0123(8)
H(7)	2*e*	1	0.765(14)	¼	0.979(11)	0.07(3)*

Notes: *The temperature factor has the form exp(-T) where $T = 8\pi^2 U(\sin(\theta)/\lambda)^2$ for isotropic atomic displacements.

Table 4. Atoms, site occupancies, fractional atom coordinates (Å), and equivalent isotropic displacement parameters ($Å^2$) for the studied canosioite crystal

Table 5.

This is a 'preproof' accepted article for Mineralogical Magazine.
This version may be subject to change during the production process.
DOI: 10.1180/minmag.2016.080.097

site	U_{11}	U_{22}	U_{33}	U_{12}	U_{13}	U_{23}
T(1)	0.0077(3)	0.0085(4)	0.0067(3)	0	0.0017(2)	0
T(2)	0.0078(3)	0.0062(3)	0.0062(3)	0	0.0031(2)	0
M	0.0100(4)	0.0067(4)	0.0062(4)	0.0004(3)	0.0025(3)	0.0006(3)
A(1)	0.01548(17)	0.0234(2)	0.01428(18)	0	0.00889(13)	0
A(2)	0.00996(15)	0.01118(16)	0.00970(15)	0	0.00415(11)	0
O(1)	0.0185(13)	0.0121(13)	0.0134(12)	0.0001(11)	0.0071(10)	−0.0009(11)
O(2)	0.0122(17)	0.027(2)	0.0141(18)	0	0.0025(14)	0
O(3)	0.021(2)	0.034(2)	0.028(2)	0	0.0189(18)	0
O(4)	0.0172(13)	0.0136(13)	0.0190(13)	0.0004(11)	0.0047(11)	0.0014(11)
O(5)	0.020(2)	0.063(3)	0.023(2)	0	0.0175(18)	0
O(6)	0.0151(17)	0.0188(19)	0.0151(18)	0	0.0043(14)	0
O(7)	0.0131(17)	0.0098(17)	0.0137(17)	0	0.0047(14)	0

Notes: *The temperature factor has the form exp(-T) where $T = 2\pi^2\Sigma_{ij}(h(i)h(j)U(i,j)a^*(i)a^*(j))$

Table 5. Anisotropic displacement parameters* for canosioite (Å)

This is a 'preproof' accepted article for Mineralogical Magazine.
This version may be subject to change during the production process.
DOI: 10.1180/minmag.2016.080.097

Table 6.

T(1)–O(4) (×2)	1.679(3)	*A*(1)–O(4) (×2)	2.672(3)
–O(5)	1.679(4)	–O(2)	2.713(4)
–O(6)	1.775(4)	–O(5)	2.775(4)
<*T*(1)–O>	1.703	–O(1) (×2)	2.779(3)
V(Å^3)	2.529	–O(6)	2.939(4)
σ^2*	3.916	–O(3)	3.147(4)
λ*	1.002	<*A*(1)–O>	2.810
		V(Å^3)	33.055
T(2)–O(3)	1.649(4)		
–O(2)	1.665(4)	*A*(2)–O(3)	2.689(4)
–O(1) (×2)	1.719(3)	–O(4) (×2)	2.706(3)
<*T*(2)–O>	1.688	–O(4) (×2)	2.885(3)
V(Å^3)	2.466	–O(7)	2.925(4)
σ^2*	1.485	–O(1) (×2)	2.938(3)
λ*	1.001	–O(2)	2.989(4)
		–O(2) (×2)	3.130(9)
M–O(7) (×2)	1.967(2)	<*A*(1)–O>	2.902
–O(1) (×2)	1.990(3)	*V*(Å^3)	54.596
–O(6) (×2)	2.106(3)		
<*M*–O>	2.021	O(7)–H(7)	0.787(10)
V(Å^3)	10.877	O(7)···O(5)	2.787(6)
σ^2*	24.728	O(5)···H(7)	2.017(10)
λ*	1.009	O(7)-H-O(5)	166(9)°

Notes: *Mean quadratic elongation (λ) and the angle variance (σ^2) were computed according to Robinson *et al*. (1971)

Table 6. Main interatomic distances (Å) and geometrical parameters for canosioite. The mean quadratic elongation (λ) and the angle variance (σ^2) according to Robinson *et al*. (1971)

This is a 'preproof' accepted article for Mineralogical Magazine.
This version may be subject to change during the production process.
DOI: 10.1180/minmag.2016.080.097

Table 7.

site	*T*(1)	*T*(2)	*M*	*A*(1)	*A*(2)	*H*(7)	Σ
O(1)		1.147 x2↓	0.510 x2↓	0.259 x2↓	0.168 x2↓		2.084
O(2)		1.325		0.310	0.147		1.882
					0.100 x2↓ x2→		
O(3)		1.384		0.169	0.330		1.883
O(4)	1.277 x2↓			0.346 x2↓	0.315 x2↓		2.131
					0.194 x2↓		
O(5)	1.277			0.262		0.176	1.714
O(6)	0.987		0.374 x2↓ x2→	0.097			1.832
O(7)			0.543 x2↓ x2→		0.174	0.793	2.053
b.v.	4.816	5.002	2.854	2.048	2.205	0.969	17.894/17.794↑
Agg. ch.	5.000	5.000	2.941	2.000	2.000	1.000	

Note: anion sites coordination reported only for coordination other than 3.

Table 7. Bond valence calculations for braccoite (Brown, 1981)

This is a 'preproof' accepted article for Mineralogical Magazine.
This version may be subject to change during the production process.
DOI: 10.1180/minmag.2016.080.097

Table 8.

Brackebuschite supergroup, $A1^{2+}\,A2^{2+}\,[^{VI}M^{3+}_{x},{}^{VI}M^{2+}_{1-x}]\,[^{IV}(T^{5+}_{x},T^{6+}_{1-x})O_4]_2\,(X^{-},X)$

Arsenbrackebuschite group *dominant at* ***T*** **= As**	**Brackebuschite group** *dominant at* ***T*** **= V**	**Goedkenite group** *dominant at* ***T*** **= P**	**Tsumebite group** *dominant at* ***T*** **= (P or As) + (S or V)**
Arsenbrackebuschite [1][2]	Brackebuschite[6][8][9][10][11]	Bearthite[18][19][20]	Arsentsumebite [3][4][5]
$Pb_2Fe^{3+}(AsO_4)_2(OH,H_2O)$	$Pb_2Mn^{3+}(VO_4)_2(OH)$	$Ca_2Al(PO_4)_2(OH)$	$Pb_2Cu[(AsO_4)(SO_4)](OH)$
Feinglosite [7]	Calderónite* [12]	Goedkenite [24]	Bushmakinite [21][22][23]
$Pb_2Zn(AsO_4)_2(OH,H_2O)$	$Pb_2Fe^{3+}(VO_4)_2(OH)$	$Sr_2Al(PO_4)_2(OH)$	$Pb_2Al[(PO_4)(VO_4)](OH)$
Grandaite [29]	Gamagarite [13][14][15]		Ferribushmakinite [30]
$Sr_2Al(AsO_4)_2(OH)$	$Ba_2Fe^{3+}(VO_4)_2(OH,H_2O)$		$Pb_2Fe^{3+}[(PO_4)(VO_4)](OH)$
Canosioite [31]	Heyite* [16][30]		Tsumebite [10][25][25][25][28]
$Ba_2Fe^{3+}(AsO_4)_2(OH)$	$Pb_5Fe^{2+}{}_2(VO_4)_2O_4$		$Pb_2Cu[(PO_4)(SO_4)](OH)$
	Tokyoite [17]		
	$Ba_2Mn^{3+}(VO_4)_2(OH)$		

Refs: [1] Abraham *et al*. (1978); [2] Hofmeister and Tillmanns (1978); [3] Vésignié, J.P.L. (1935); [4] Bideaux *et al*. (1966); [5] Zubkova *et al.* (2002); [6] Brackebusch *et al*. (1883); [7] Clark *et al*. (1997); [8] Rammelsberg (1880); [9] Donaldson and Barnes (1955); [10] Fanfani and Zanazzi (1967); [11] Foley *et al*. (1997); [12] González del Tánago *et al*. (2003); [13] de Villiers (1943); [14] Harlow *et al*. (1984); [15] Basso *et al*. (1987); [16] Williams (1973); [17] Matsubara *et al*. (2004); [18] Brunet *et al*. (1993); [19] Brunet and Chopin (1995); [20] Roth (2007); [21] Pekov *et al*. (2002); [22] Yakubovich *et al*. (2002); [23] Pekov (2007); [24] Moore *et al*. (1975); [25] Rosický (1912); [26] Busz (1912); [26] Spencer (1913); [28] Nichols (1966); [29] Cámara *et al*. (2014); [30] Kampf *et al*. (2015); [31]this study; * recent examination on the holotype specimen (BM1972,194) has confirmed the structural correspondence of heyite and calderónite (Kampf *et al*., 2015).

Table 8. The brackebuschite supergroup (references are given in brackets)

DOI: 10.1180/minmag.2016.080.097

This is a 'preproof' accepted article for Mineralogical Magazine.
This version may be subject to change during the production process.
DOI: 10.1180/minmag.2016.080.097

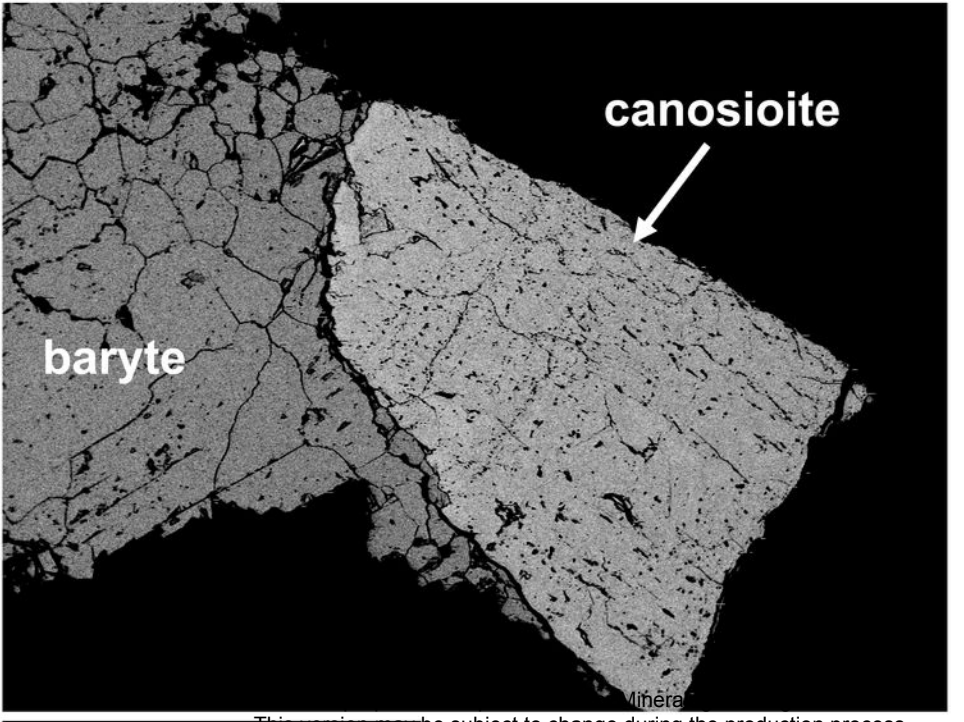

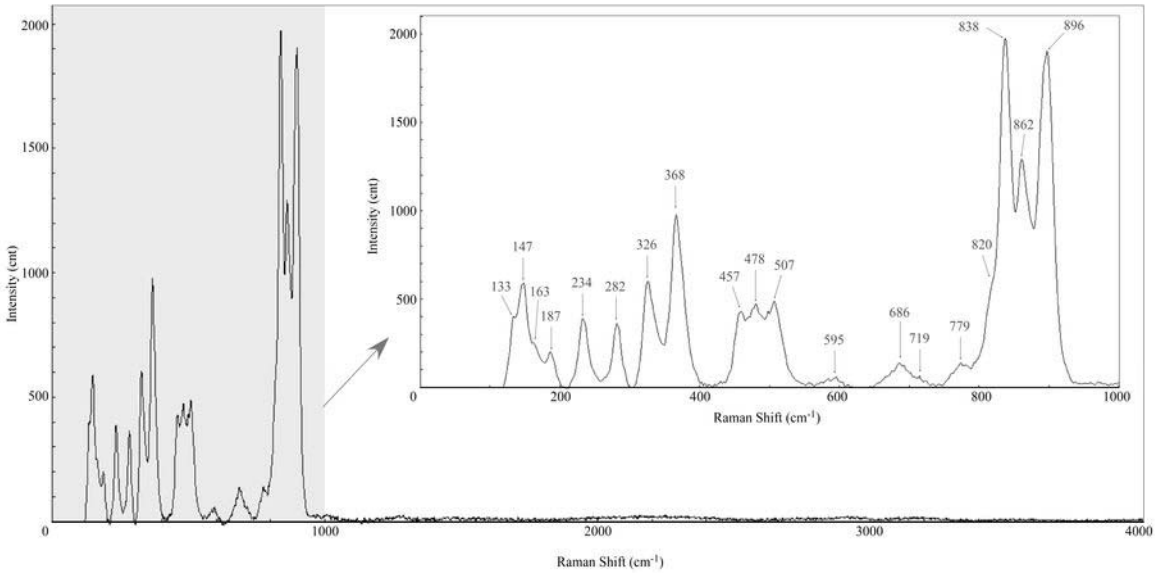

This is a 'preproof' accepted article for Mineralogical Magazine.
This version may be subject to change during the production process.
DOI: 10.1180/minmag.2016.080.097

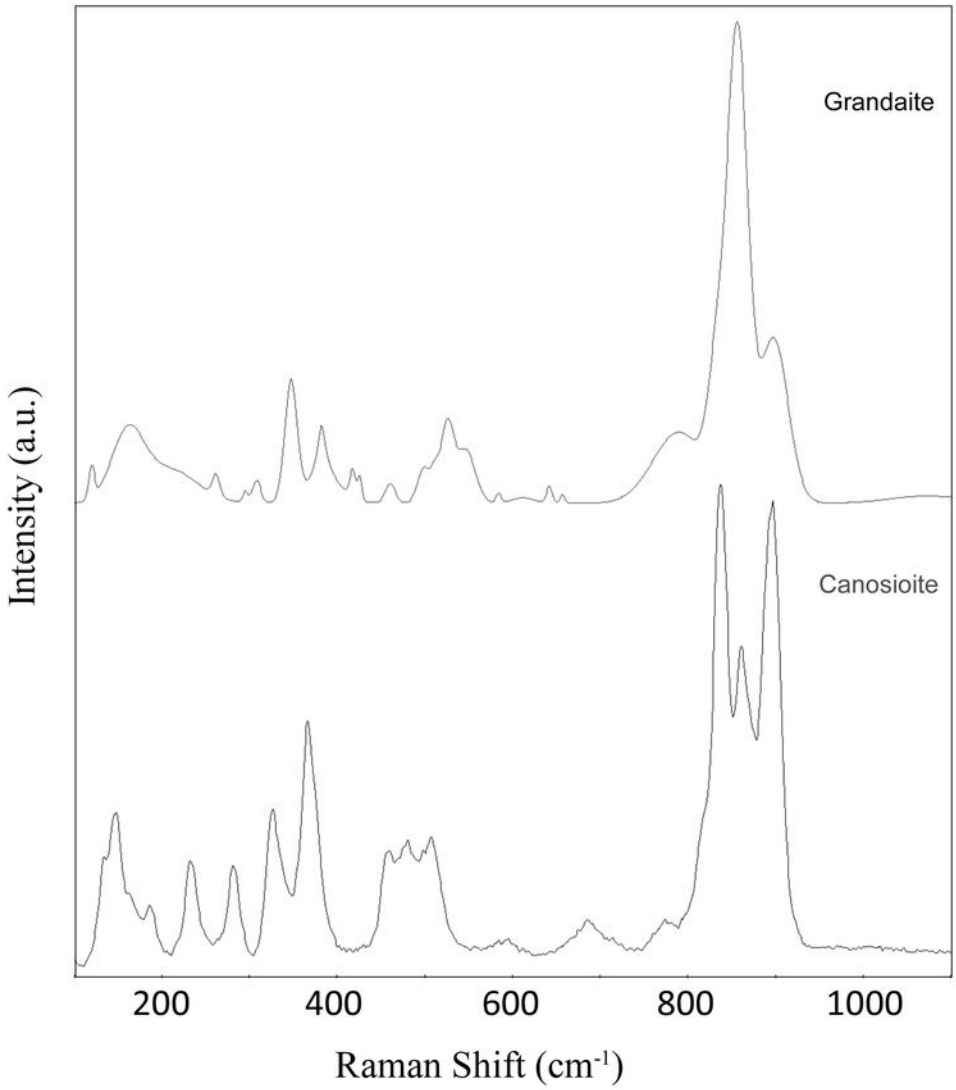

This is a 'preproof' accepted article for Mineralogical Magazine.
This version may be subject to change during the production process.
DOI: 10.1180/minmag.2016.080.097

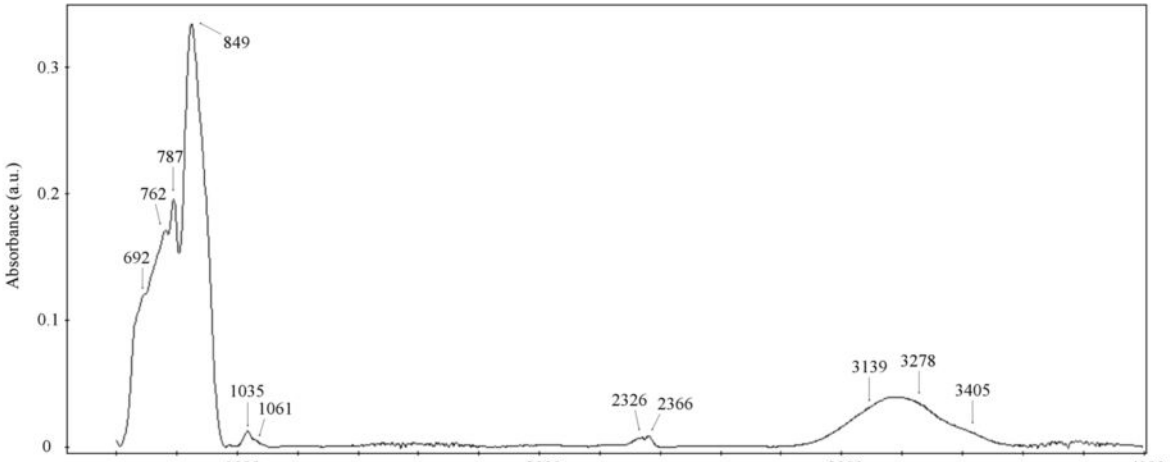

DOI: 10.1180/minmag.2016.080.097

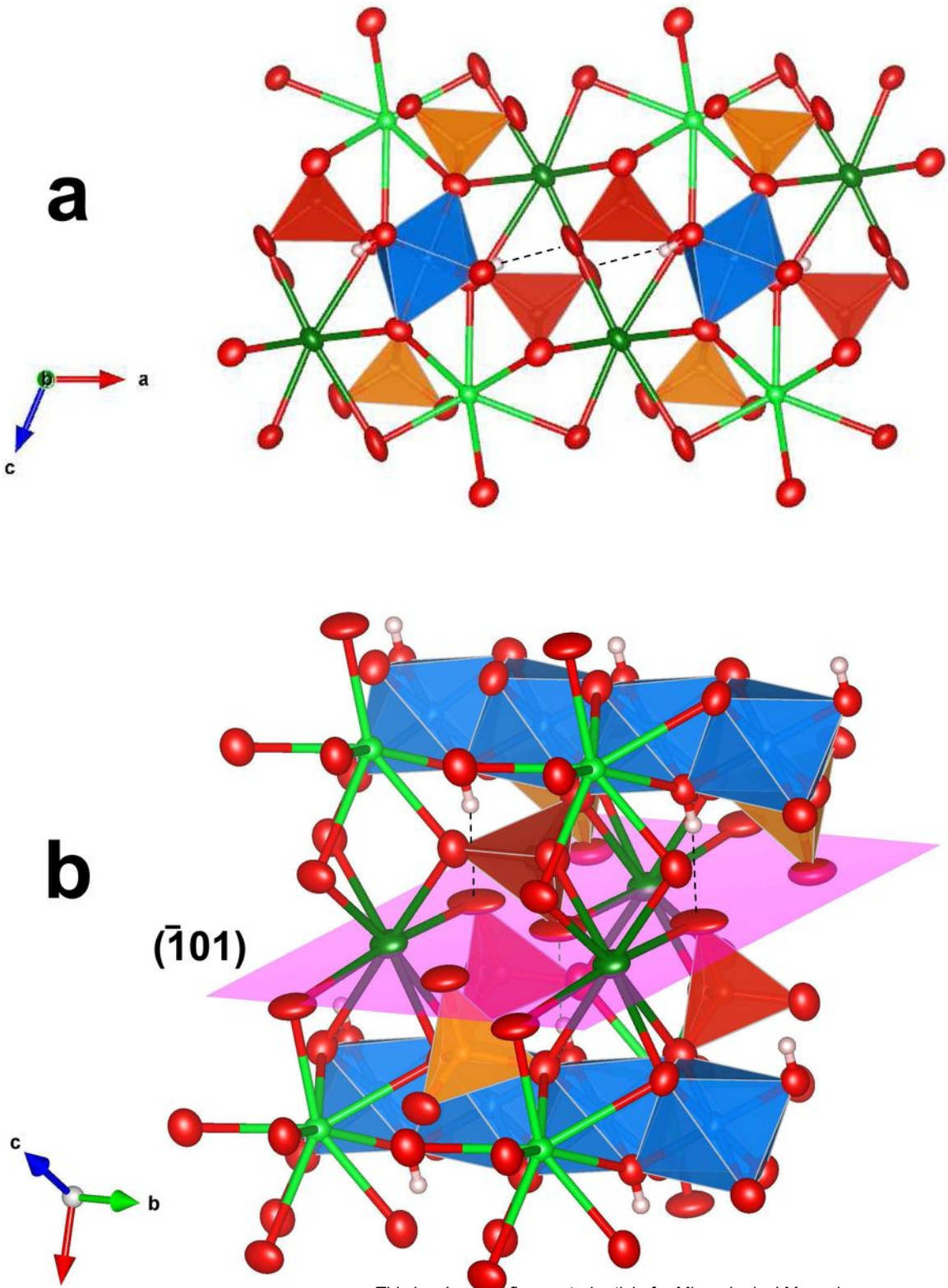

This is a 'preproof' accepted article for Mineralogical Magazine.
This version may be subject to change during the production process.
DOI: 10.1180/minmag.2016.080.097